# Large-Amplitude Motions of Form III of Isotactic Poly(4-methyl-1-pentene) Crystallites Prior to Crystal−Crystal Transformation

**Toshikazu Miyoshi,*,† Ovidiu Pascui,‡ and D. Reichert*,‡**

*Research Center of Macromolecular Technology, National Institute of Advanced Industrial Science and Technology (AIST), Tokyo-Water-front, 2-41-6 Aomi, Kohto-ku, Tokyo, 135-0064, Japan, and Fachbereich Physik, Martin-Luther-Universität Halle-Wittenberg, 06108 Halle, Germany*

*Received April 7, 2004*
*Revised Manuscript Received June 15, 2004*

## Introduction

Solid-state crystal−crystal transformations frequently occur in crystalline polymers, spontaneously[1] or under specific treatments, for example, mechanical stretching.[2] Crystal−crystal transformations accompany changes in the molecular structure such as conformation, packing, or both. These structural changes require internal rotations around chemical bonds, lateral displacements, translations, and rotations of the polymer chains in the restricted space. In most of the crystal−crystal transformations, the chirality of the helix is preserved due to the spatial restrictions imposed by the lattice.[1] These structural changes are commonly discussed on the basis of static crystalline structures before and after the transformations; however, it is often expected that molecular dynamics plays an important role for the crystal−crystal transformation.[2] Therefore, it is interesting to investigate the molecular dynamics in polymer crystallites prior to the transformation.[3,4] Solid-state 2D exchange NMR experiments provide detailed information about the motional geometry and kinetic parameters of polymers[5] and have revealed that the polymer chains in the crystalline region perform large-amplitude motions in the mechanical $\alpha_c$-relaxation process.[6−10] It has been proven that such dynamical processes are directly related to mechanical properties, drawability of polymer materials, and the crystallization process.[5,6] Static 2D exchange NMR is a powerful tool for dynamical studies; however, for polymers with more than one chemically inequivalent carbon in the monomeric unit, it requires isotope labeling in order to achieve molecular resolution. A number of 1D-MAS exchange methods have been developed to avoid this problem.[11−16]

Very recently, we successfully characterized the side- and main-chain dynamics of form I of isotactic poly(4-methyl-1-pentene) crystallites in natural abundance.[17,18] We utilized centerband-only of detection of exchange (CODEX)[14,15] NMR that we improved by adding a rotor synchronized $T_{1\rho}$ filter. It was found that form I chains perform helical jump motions at temperatures slightly lower than the glass transition temperature ($T_g$ = 304 K) and that no independent slow side-chain dynamics exists. The temperature dependence of the correlation times obeys WLF behavior while so far, the crystalline dynamics in several systems was described in terms of the Arrhenius function.[7,9,10] The WLF behavior for the *i*P4M1P crystallites was interpreted by the amorphous constraints around $T_g$.

*i*P4M1P crystallites show a complicated polymorphic behavior of forms II−V, depending on the crystallization condition such as pressure, solvent, and thermal history.[19−21] Forms II, III, and V spontaneously transform into the stable form I with increasing temperature.[20−22] Rosa et al. determined the crystalline structure of form III.[23] They showed that four $4_1$ helixes are packed into a tetragonal lattice with a density of 0.790 g/cm$^3$, which is smaller than that of form I (0.828 g/cm$^3$). In the present work, we investigate the side- and main-chain dynamics of form III of *i*P4M1P by 1D-MAS exchange NMR in natural abundance. We will characterize type and time scale of molecular dynamics in unstable form III prior to the crystal−crystal transformation into form I.

## Experiments

**Sample.** *i*P4M1P with an average molecular weight of $M_w$ = 180 000 was purchased from Poly Science Co. Ltd. The virgin sample was dissolved into semidilute toluene solvent (0.25 wt %) and was kept at least for 10 h at 378 K. Subsequently, the solution was rapidly cooled in air[19,20] and dried under vacuum for 1 day at room temperature, resulting in the form III-rich sample. The crystallinity and polymorphism of the sample were characterized by wide-angle X-ray diffraction (WAXD). The X-ray diffractometor (Rigaku Rint 2500, VH/PC) utilized Cu Kα radiation (40 kV, 300 mA). The peak analysis revealed that form III-rich sample has a crystallinity of 73% and includes form I of 4%.[19−21] In our previous works, we characterized crystallinity of the form I-rich sample, by DSC, which was obtained by transformation of the form III-rich sample in the present work. The determined crystallinity for form III-rich sample agrees well with that for the form I-rich sample (69%).[17,18]

**NMR Measurements.** The $^{13}$C CPMAS and mixing time ($t_{mix}$) dependence (exchange decay) for CODEX experiments were carried out on a BRUKER AVANCE 300 spectrometer, equipped with a 7 mm VT CPMAS NMR probe. The $^{13}$C carrier frequency is 75.6 MHz. The MAS frequency was set to 3000 ± 3 Hz. The 90° pulses for $^1$H and $^{13}$C are 4.5−5.0 $\mu$s. The recycle delay and cross-polarization (CP) time are 2 s and 1 ms, respectively. High-power $^1$H CW or TPPM decoupling is used for the detection period. The chemical shift is referred to CH signal of adamantane at 29.5 ppm as an external reference. The temperature in the probe was calibrated using the temperature-dependent chemical shift of $^{207}$Pb of $Pb(NO_3)_2$.[24,25] The $T_{1\rho c}$ measurements were carried out under a spin-locking field strength of 50 kHz. 2D exchange NMR spectra were obtained by the traditional three-pulse scheme.[5] 320 slices with a dwell time of 140 $\mu$s were acquired along the $t_1$ dimension. The TPPI procedure[26] was used in the $t_1$ dimension.

A rotor synchronized $^{13}$C $T_{1\rho}$ relaxation filter was incorporated into the CODEX program to suppress the broad and minor amorphous signals. The $^{13}$C $T_{1\rho}$ relaxation filter lengths were 18, 15, 12, 10, 7, 2, and 2 ms at 258, 286, 292, 299, 305, 311, and 316 K, respectively. The MAS frequency was again set to 3000 ± 3 Hz. The 180° pulse length for $^{13}$C channel is 15 $\mu$s. CW and TPPM decoupling were applied during evolution and detection periods, respectively. The radio-frequency field strength for CW decoupling during the $^{13}$C 180° pulse cycles was set to 80 kHz. To suppress drift of NMR spectrometer, the reference and exchange experiments were obtained alternatively after every 128 transients. Totally, each spectrum was

† Recerch Center of Macromolecular Technology, AIST.
‡ Martin-Luther-Universität Halle-Wttenberg.
* To whom corresponding author should be addressed. T.M.: e-mail t-miyoshi@aist.go.jp; Tel +81-298-61-9392; Fax +81-298-61-6243. D.R.: e-mail reichert@physik.uni-halle.de; Tel +49-345-55-25593; Fax +49-345-55-27161.

10.1021/ma049323w CCC: $27.50 
Published on Web 07/27/2004

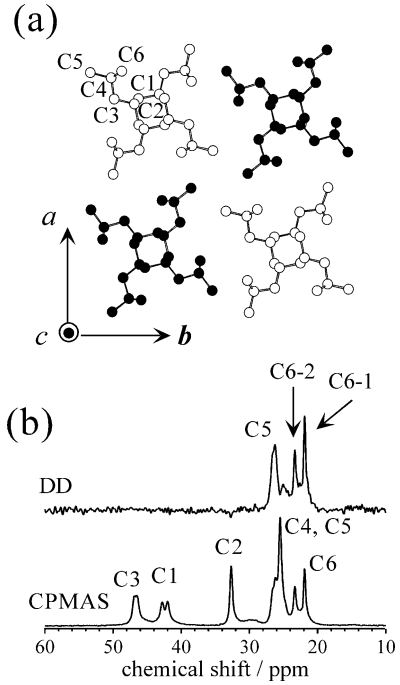


**Figure 1.** (a) Crystalline structure of form III of *i*P4M1P as determined by WAXD.[23] Carbon atoms are represented by open (left-handed chain) and filled (right-handed chain) circles. (b) $^{13}$C CPMAS NMR spectra of form III-rich sample with and without dipolar dephasing time of 100 $\mu$s. We denote the two signals in the C6 doublet at 22.1 and 23.7 ppm as C6-1 and C6-2, respectively.

obtained by accumulating 1024 transients. The total experimental time for mixing-time ($t_{mix}$) dependence with mixing times up to 10 s was about 40 h.

The evolution-time ($Nt_r$) dependence for CODEX experiment (CODEX CSA-recoupling curves) was measured on a Varian Inova 400 equipped with a standard Varian 7 mm VT-CPMAS probe. The $^{13}$C carrier frequency was 100.5 MHz. The MAS frequency is set to 5500 ± 3 Hz. The lengths of $^{13}$C 90° and $^{1}$H 90° pulses were 3.8 and 4.1 $\mu$s, respectively. The mixing time was set to 107 ms. $^{1}$H CW decoupling with field strength of 65 kHz was applied. The full experimental time for a CSA-evolution time experiment was about 12 h.

## Results and Discussion

The $^{13}$C NMR spectra of crystalline polymers commonly feature narrow line widths due to well-defined packing and conformation. Therefore, the observed line shape and isotropic chemical shift easily provide information about the crystalline structures and dynamics. In form III of *i*P4M1P, two right-handed and two left-handed helixes are packed in a tetragonal lattice with $a = b = 19.38$ Å and $c = 6.98$ Å.[23] In Figure 1a, the atoms of right- and left-handed polymer chains are represented by filled and open circles, respectively. Each molecule forms a uniform $4_1$ helix and is surrounded by four opposite-handed chains. Figure 1b shows $^{13}$C CPMAS NMR spectra of the form III-rich sample with and without dipolar dephasing (DD) at 243 K. In the DD experiment, one can selectively observe the $^{13}$C signals with weak $^{1}$H−$^{13}$C dipolar coupling, and the spectrum shows the two methyl signals of C5 and C6 in Figure 1b. The observed chemical shift difference between C5 and 6 signals is attributed to the $\gamma$ gauche effect.[27,28] The C6 carbon has a torsion angle of 74° with respect to the main-chain CH carbon (C2) in the $\gamma$ position, whereas C5 carbon makes an angle of −174° with respect to C2 in the $\gamma$ position. Another interesting point is the doublet line shape for the main-chain $CH_2$ (C1), side-chain $CH_2$ (C3), and C6 carbons. Among them, C6 carbon shows the largest separation of 1.6 ppm at 243 K. Such a splitting can be explained by the packing structure of two independent polymer chains in a tetragonal lattice.[22,23]

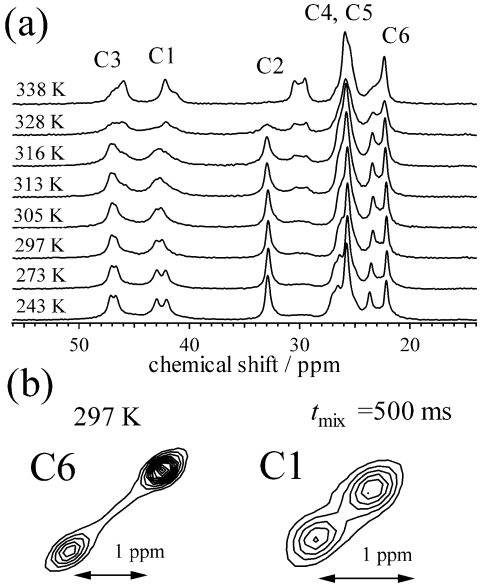


**Figure 2.** (a) $^{13}$C CPMAS NMR spectra of a form III-rich sample at various temperatures. (b) $^{13}$C 2D exchange NMR spectra of the C1 and C6 regions with $t_{mix} = 500$ ms at 297 K.

Figure 2 shows $^{13}$C CPMAS NMR spectra for the form III-rich sample as a function of temperature. The separations of the C1, C3, and C6 doublet signals become smaller with increasing temperature, and the C1 and C3 signals show line broadening. As a result, the doublet signals of the C1 and C3 signals change to the single ones above 305 K. Above 313 K, the transformation from form III into form I is observed through the C2 signal. Since the C2 signal has significantly different chemical shifts in the different forms I and III, the line shape and chemical shift of the C2 signal are good indicators of the structural and dynamics changes due to the transformation. Below 338 K, the chemical shift of the C2 signal is almost invariant. On the other hand, the line width shows motional broadening, indicating that segmental motions occur in form III crystallites prior to the transformation.

2D-MAS exchange NMR spectrum with $t_{mix} = 500$ ms was taken at 297 K. This temperature is slightly lower than the temperature at which the doublets of the C1 and C3 signals change to the single resonances. The 2D spectra of the C1 and C6 signals with $t_{mix} = 500$ ms are shown in Figure 2b. It is obvious that no cross-peaks between the doublet signals are apparent, even upon increase of $t_{mix}$ up to 2 s (data are not shown). These results are consistent with the signal assignments that the observed doublet signals arise from right- and left-handed chains; these physically cannot interchange with each other. Therefore, the observed line shape changes of the C1 and C3 signals and the decrease of the chemical shift difference of the C6 signals indicate changes in the packing structure due to molecular dynamics.

We now advance to CODEX-NMR experiments to investigate the motional geometry of the polymer chains in the crystalline region. CODEX NMR can detect reorientation of the chemical shift anisotropy (CSA)

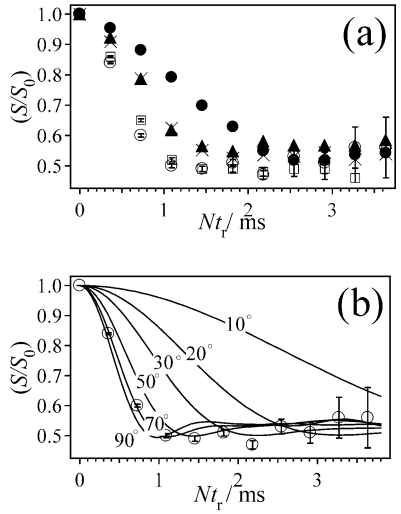


**Figure 3.** CODEX $Nt_r$ dependence (recoupling curves) of C1 (○), C2 (●), C3 (□), C6-1 (▲), and C6-2 (×) for form III of *i*P4M1P with $t_{mix} = 107$ ms under a MAS frequency of 5500 ± 3 Hz at 311 K. The error bars were determined from the spectral signal-to-noise ratio. (b) $Nt_r$ dependence of C1 signal and simulated curves for rotational jump motions with jump angles of 10°, 20°, 30°, 50°, 70°, and 90° around its helical axes in a uniform $4_1$ helix.

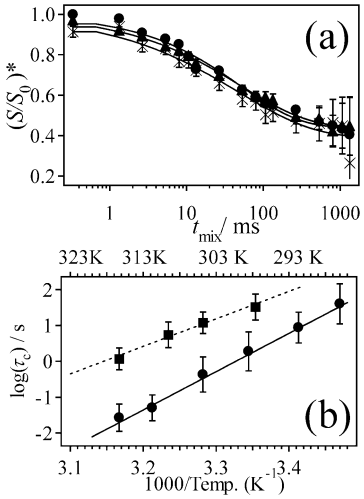


**Figure 4.** (a) $t_{mix}$ dependence of $(S/S_0)^*$ intensities (exchange decays) for C2 (●) and C6-1 (▲) and C6-2 (×) for $Nt_r = 2.7$ ms at 311 K, where $(S/S_0)^* = (S/S_0)/(S/S_0)_{SD}$; $(S/S_0)_{SD}$ was obtained at reasonably low temperatures where the molecular dynamics is frozen (258 K). The solid curves are best fits to the experimental data using the equation $(S/S_0)^* = 1 - p(1 - \exp(-t_{mix}/\langle\tau_c\rangle)^\beta)$. (b) Arrhenius diagram of the correlation times for helical jump motions of form III (●) and of form I[18] (■) of *i*P4M1P crystallite obtained by CODEX. In both forms, $\langle\tau_c\rangle$ values were obtained from the C2 signal. The bars mean the distribution widths for the $\langle\tau_c\rangle$ values, assuming a log−Gaussian distribution.[32] The solid and broken lines in form III (●) and form I (■) show Arrhenius curves with best-fitted parameters of $E_a = 215 \pm 10$ and $147 \pm 17$ kJ/mol.

tensor due to molecular dynamics.[14,15] Therefore, we can obtain geometrical and kinetic parameters from the main- and side-chain signal intensities. Figure 3a shows the $Nt_r$ dependence (CSA-recoupling curve) of the CODEX signal intensities of $(S/S_0)$ of all the resolved signals of form III with a $t_{mix} = 107$ ms at 311 K, where $S$ and $S_0$ denote the signal intensities for exchange and reference spectra, respectively. All signals show steep decays in the initial periods. If the side chains perform independent motions on the same time scale, the plateau values of the side-chain signals would be smaller than those of the main chain. Actually, the front of the side-chain groups, C6, show similar plateau values (C6-1 0.56, C6-2 0.54) with those of the main-chain C1 (0.56) and C2 (0.55) signals. Therefore, it is concluded that there is no additional slow side-chain dynamics in both right- and left-handed chains in form III crystallites. This is consistent with the side- and main-chain dynamics in form I.[17,18]

We simulated the CODEX $Nt_r$ dependence of the C1 signal, which requires knowledge about the CSA tensor direction and principal axes values. The latter were determined to be 66 ppm ($\sigma_{11}$), 44 ppm ($\sigma_{22}$), and 20 ppm ($\sigma_{33}$).[29] We use common CSA directions for the −C−$CH_2$−C− moiety[30,31] as follows: $\sigma_{22}$ is parallel to the direction bisecting the $CH_2$ angle, $\sigma_{33}$ is orthogonal to the $CH_2$ plane, and $\sigma_{11}$ is orthogonal both to $\sigma_{22}$ and $\sigma_{33}$ directions. The Euler angles describe the geometry of molecular motions by CSA tensor orientations before and after $t_{mix}$. These orientations were obtained from the crystalline structures, where we choose the helical axis as $Z$-axis in reference frame.[5] The solid curves in Figure 3b show calculated CODEX recoupling curves for different hypothetical jump angles around its helical axis. Increase of the jump angle results in a steeper decay during the initial evolution period. The simulations with jump angles of 70−90° reproduce the experimental data. In the $4_1$ helix, the theoretical jump angle between the neighboring sites is 90°. Therefore, the comparison of simulation and experimental result indicates that form III chains perform helical jumps before the transformation. This is in agreement with previous solid-state NMR investigations of several other polymers, which spontaneously undergo crystal−crystal transformations. It was shown that poly(tetrafluoroethylene) (PTFE) also shows rotational motions around its chain axis before the transformation[3] and that form III of isotactic poly(1-butene) (*i*PB) features helical jumps prior to the transformation.[4] These types of motions are typical for the $\alpha_c$-relaxation of several flexible crystalline polymers.[5−10,17,18]

As already shown, the $Nt_r$ experiments are dominated by helical jump motions. In $t_{mix}$ experiments, we measured the $t_{mix}$ dependencies (exchange decays) $(S/S_0)^*$ of the C2, C6-1, and C6-2 signals with sufficient signal-to-noise ratios, compared to those of C1 and C3, as shown in Figure 1b, where $(S/S_0)^*$ includes pure kinetic parameters after spin-diffusion correction.[16,17,32] Figure 4a shows $t_{mix}$ dependence of the $(S/S_0)^*$ intensities of C2, C6-1, and C6-2 at 311 K. It is obvious that they are all very similar. The exchange curves are fitted to the equation of $(S/S_0)^* = 1 - p(1 - \exp(-t_{mix}/\langle\tau_c\rangle)^\beta)$,[14,15,17] where $p$ is related to the number of the available sites, $m$, by the dynamic process, $p = (m - 1)/m$, $\langle\tau_c\rangle$ is the mean value of the correlation times, and $\beta$ can be recalculated into the distribution width of a log−Gaussian distribution of correlation times.[32] The solid curves in Figure 4a are best fits to the experimental data. While C2 ($p = 0.56 \pm 0.02$, $\langle\tau_c\rangle = \langle 50.6 \pm 7.9\rangle$ ms, $\beta = 0.56 \pm 0.05$) tells about the average dynamics between the right- and left-handed chains, we can monitor the chain dynamics in two independent helixes in the lattice from the two C6 signals. The best-fitted parameters of C6-1 ($p = 0.61 \pm 0.03$, $\langle\tau_c\rangle = \langle 47.9 \pm 16.5\rangle$ ms, $\beta = 0.44 \pm 0.06$) are well consistent with those of C6-2 ($p = 0.56 \pm 0.03$, $\langle\tau_c\rangle = \langle 51.1 \pm 5.4\rangle$ ms, $\beta = 0.49 \pm 0.02$). From this evidence, the right- and left-handed chains perform helical jumps with consistent kinetic

parameters. The obtained $p$ values with 0.56−0.61 indicate that 75−81% of the segments participate in the helical jumps. The $\beta$ values can be recalculated[32] into a distribution width of about 1.4−1.7 frequency decades. Such a dynamic heterogeneity in time is observed even in the other polymer crystallites.[7,14,18] The observed lineshape changes of the C1, C3, and C6 carbons with increasing temperature, as shown in Figure 2a and dynamic analysis by CODEX, indicate that packing relation between the neighboring chains changes due to dynamics of the helixes.

In Figure 4b, we plotted $\langle\tau_c\rangle$ values of the helical jumps of form III, obtained from the C2 signal as a function of temperature (circles). Actually, it is difficult to judge whether the $\langle\tau_c\rangle$ values of helical jump motions in form III obey an Arrhenius or not, due to the limited temperature range. We simply apply Arrhenius analysis to the present data. The best fitting value is $E_a = 215 \pm 10$ kJ/mol. This is much larger than the previously reported values in other crystalline polymers such as PE (125 kJ/mol),[7] POM (80 kJ/mol),[9,10] and form III of *i*PB (79 kJ/mol)[4] but comparative with the value of PTFE (200 kJ/mol).[3] However, the activation energy of crystalline dynamics depends on a number of factors such as monomer structure, helical structure, packing, lamellar thickness in the crystalline region, and amorphous and/or interfacial mobility related to $T_g$. Therefore, it is difficult to compare the activation energy of different crystalline polymers. In our previous works[17,18] we determined $\langle\tau_c\rangle$ for helical jumps of form I of *i*P4M1P in the temperature of 297−360 K. For comparison, the $\langle\tau_c\rangle$ values of the stable form I in the similar range of 297−316 K are plotted in Figure 4b (squares).[18] The previous analysis demonstrated dynamics of form I obey WLF behavior. In this limited range, we simply treat the dynamic behavior of form I by Arrhenius function with $E_a = 147 \pm 17$ kJ/mol (broken line) to compare with that of form III. To explain a substantial difference between $E_a$ values of forms I and III, we discuss the structural difference between form I-rich and form III-rich samples: The form I-rich sample was produced by the transformation of a form III-rich sample.[16,18] We thus assume that crystallinity, lamellae thickness, and $T_g$ of the form I-rich sample are similar to those of the form III-rich sample. Therefore, only the crystalline density (interchain distance and length per monomer unit along $c$ axis) between forms I (0.828 g/cm$^3$) and III (0.790 g/cm$^3$) and the amorphous immobility would influence the $\langle\tau_c\rangle$ values. For example, the $\langle\tau_c\rangle$ value for form III at 316 K is by 1.5 orders of magnitude smaller than that of form I. This is explained by the smaller density of form III as compared to that of form I. The onset temperature of helical jumps in form III which are detected by NMR ($\langle\tau_c\rangle \sim 10^2$ s) is lower (283 K, $T_g - 21$ K) than that of form I (294 K, $T_g - 10$ K), as shown in Figure 4b. This temperature difference (relative to $T_g$) suggests that the dynamics in form III is more severely restricted by the amorphous rigidity and leads to the increase in the $E_a$ value for form III.

In summary, we successfully demonstrated that the unstable form III chains perform helical jump motions and no independent slow side-chain motion prior to the crystal−crystal transformation. A similar type of large-amplitude motions was observed in other systems, for example, form III of *i*PB[4] and PTFE,[3] which spontaneously undergo crystal−crystal transformations, and form I of *i*P4M1P[17,18] and other flexible semicrystalline polymers[5−10] in the $\alpha_c$-relaxation temperature. It is, therefore, concluded that the large-amplitude motions around their helical axes play important roles for the spontaneous crystal−crystal transformations as well as mechanical property and crystallization process.

**Acknowledgment.** T.M. thanks NEDO (New Energy and Industrial Technology Development Organization) in the framework of Nanostructure Polymer Project. O.P. and D.R. thank the Deutsche Forschungsgemeinschaft DFG in the frame of SFB 418 for financial support. We thank Dr. Y. Li (AIST) for performing the WAXD measurements.

## References and Notes

(1) Lotz, B.; Mathieu, C.; Lovinger, A. J.; De Rosa, C.; Ruiz, O.; Auriemma, F. *Macromolecules* **1998**, *31*, 9253−9257.
(2) Saraf, F. R.; Porter, R. S. *J. Polym. Sci., Part B: Polym. Phys.* **1988**, *26*, 1049−1057.
(3) Vega, A. J.; English, A. D. *Macromolecules* **1980**, *13*, 1635−1647.
(4) Miyoshi, T.; Hayashi, S.; Imashiro, F.; Kaito, A. *Macromolecules* **2002**, *35*, 2624−2632.
(5) Schmidt-Rohr, K.; Spiess, H. W. *Multidimensional Solid-State NMR and Polymers*; Academic Press: London, 1994.
(6) Hu, W. G.; Schmidt-Rohr, K. *Acta Polym.* **1999**, *50*, 271−285.
(7) Hu, W. G.; Boeffel, C.; Schmidt-Rohr, K. *Macromolecules* **1999**, *32*, 1611−1619.
(8) Schaefer, D.; Spiess, H. W.; Suter, U. W.; Fleming, W. W. *Macromolecules* **1990**, *23*, 3431−3439.
(9) Kentgens, A. P. M.; de Boer, E.; Veeman, W. S. *J. Chem. Phy.* **1987**, *87*, 6859−6866.
(10) Hagemeyer, A.; Schmidt-Rohr, K.; Spiess, H. W. *Adv. Magn. Reson.* **1989**, *13*, 85−130.
(11) Gerardy-Montouilout, V.; Malveau, C.; Tekely, P.; Olender, Z.; Luz, Z. *J. Magn. Reson.* **1996**, *123*, 7−15.
(12) Reichert, D.; Zimmermann, H.; Tekely, P.; Olender, Z.; Luz, Z. *J. Magn. Reson.* **1997**, *125*, 245−258.
(13) Reichert, D.; Hempel, G.; Luz, Z.; Tekely, P.; Schneider, H. *J. Magn. Reson.* **2000**, *146*, 310−320.
(14) deAzevedo, E. R.; Hu, W. G.; Bonagamba, T. J.; Schmidt-Rohr, K. *J. Am. Chem. Soc.* **1999**, *121*, 8411−8412.
(15) deAzevedo, E. R.; Hu, W. G.; Bonagamba, T. J.; Schmidt-Rohr, K. *J. Chem. Phys.* **2000**, *112*, 8988−9001.
(16) Reichert, D.; Pascui, O.; Bonagamba, T. J.; deAzevedo, E. R.; Schmidt, A. *Chem. Phys. Lett.* **2003**, *380*, 583−588.
(17) Miyoshi, T.; Pascui, O.; Reichert, D. *Macromolecules* **2002**, *35*, 7178−7181.
(18) Miyoshi, T.; Pascui, O.; Reichert, D. Submitted to *Macromolecules*.
(19) Charlet, G.; Delmas, G.; Revol, F. J.; Manley, J. St. *Polymer* **1984**, *25*, 1613−1618.
(20) Charlet, G.; Delmas, G. *Polymer* **1984**, *25*, 1619−1625.
(21) Lopez, L.; Wilkes, G. L.; Stricklen, P. M.; White, S. A. *J. Macromol. Sci. C* **1992**, *32*, 301−406.
(22) De Rosa, C.; Capotani, D.; Cosco, S. *Macromolecules* **1997**, *30*, 8322−8331.
(23) De Rosa, C.; Borriello, A.; Venditto, V.; Corradini, P. *Macromolecules* **1994**, *27*, 3864−3868.
(24) Bielecki, A.; Burum, D. P. *J. Magn. Reson. A* **1995**, *116*, 215−220.
(25) Takahashi, T.; Kawashima, H.; Sugisawa, H.; Baba, T. *Solid-State NMR* **1999**, *15*, 119−123.
(26) Redfield, A. G.; Kunz, S. D. *J. Magn. Reson.* **1975**, *19*, 250−254.
(27) Tonelli, A. E. *NMR Spectrocscopy and Polymer Microstructure: The Conformaitonal Connection*; VCH Publishers: New York, 1989.
(28) Zemke, K.; Schmidt-Rohr, K.; Spiess, H. W. *Acta Polym.* **1994**, *45*, 148−159.
(29) Liu, F. S.; Mao, J. D.; Schmidt-Rohr, K. *J. Magn. Reson.* **2002**, *155*, 15−28.
(30) Schmidt-Rohr, K.; Whilhelm, M.; Johansson, A.; Spiess, H. W. *Magn. Reson. Chem.* **1993**, *31*, 352−356.
(31) Dunbar, M. G.; Novak, B. M.; Schmidt-Rohr, K. *Solid-State NMR* **1998**, *12*, 119−137.
(32) Pascui, O.; Beiner, M.; Reichert, D. *Macromolecules* **2003**, *36*, 3992−4003.

MA049323W